frontiers in Chemistry

ORIGINAL RESEARCH
published: 12 May 2020
doi: 10.3389/fchem.2020.00349

Cl^- Doping Strategy to Boost the Lithium Storage Performance of Lithium Titanium Phosphate

Hao Luo[1†], *Yijun Tang*[2†], *Zeying Xiang*[1], *Pinghui Wu*[3*] *and Zhizhong Li*[4]

[1] School of Science, Southwest University of Science and Technology, Mianyang, China, [2] College of Science, Zhejiang University of Technology, Hangzhou, China, [3] Research Center for Photonic Technology, Fujian Key Laboratory for Advanced Micro-Nano Photonics Technology and Devices & Key Laboratory of Information Functional Material for Fujian Higher Education, Quanzhou Normal University, Fujian, China, [4] Basic Teaching Department, Neusoft Institute Guangdong, Foshan, China

OPEN ACCESS

Edited by:
Xianwen Wu,
Jishou University, China

Reviewed by:
Zhouguang Lu,
Southern University of Science and Technology, China
Kai Zhu,
Harbin Engineering University, China

***Correspondence:**
Pinghui Wu
phwu@zju.edu.cn

[†]These authors have contributed equally to this work

Specialty section:
This article was submitted to Electrochemistry, a section of the journal Frontiers in Chemistry

Received: 02 February 2020
Accepted: 03 April 2020
Published: 12 May 2020

Citation:
Luo H, Tang Y, Xiang Z, Wu P and Li Z (2020) Cl^- Doping Strategy to Boost the Lithium Storage Performance of Lithium Titanium Phosphate. Front. Chem. 8:349. doi: 10.3389/fchem.2020.00349

Because of energy storage limitations and the high demand for energy, aqueous rechargeable lithium batteries (ARLBs) are receiving widespread attention due to their excellent performance and high safety. Lithium titanium phosphate ($LiTi_2(PO_4)_3$) exhibits the potential to serve as anodes for ARLBs because it has a three-dimensional channel and a stable structure. We employed an anion (Cl^-) doping strategy to boost the lithium storage performance of $LiTi_2(PO_4)_3$. A series of $LiTi_2(PO_4)_3$/C composites doped with Cl^- on PO_4^{3-} were successfully synthesized with a sol-gel technique as anodes for ARLBs. The effects of chlorine doping with different content on the properties of $LiTi_2(PO_4)_{3-x}Cl_{3x}$/C ($x$ = 0.05, 0.10, and 0.15) were investigated systematically. The doping of chlorine in appropriate amounts did not significantly impact the main structure and morphology of $LiTi_2(PO_4)_3$/C. However, chlorine doping greatly increased the performance of $LiTi_2(PO_4)_3$/C. $LiTi_2(PO_4)_{2.9}Cl_{0.3}$/C (LCl-10) showed the best electrochemical properties. It delivered a discharge capacity of 108.5 and 85.5 mAh g^{-1} at 0.5 and 15°C, respectively, with an increase of 13.2 and 43.3 mAh g^{-1} compared to blank $LiTi_2(PO_4)_3$ (LCl). In addition, the discharge capacity of LCl-10 was maintained at 61.3% after 1,000 cycles at 5°C, implying an apparent improvement compared to LCl (35.3%). Our study showed that a chlorine-doped $LiTi_2(PO_4)_3$/C composite is a potential anode for high-performance ARLBs.

Keywords: aqueous rechargeable lithium batteries, anode, anion doping, lithium titanium phosphate, electrochemical performance

INTRODUCTION

With the advancement of modern society, environmental pollution, and energy shortages have become more serious (He et al., 2019; Jiang et al., 2019; Zhou et al., 2019; Huan et al., 2020; Li et al., 2020a,b). Electrical energy can be derived from various other forms of energy, however, as an effective means to solve these problems. The secondary battery system is a necessary device for energy conversion and storage (Wu et al., 2017; Fang et al., 2019; Yang et al., 2019; Lu et al., 2020). The needs of high-performance electronic devices and electric vehicles have motivated the rapid development of lithium-ion batteries (LIBs) in recent years. The demand for LIBs offering high energy density, low pollution, and long life has rapidly increased (Wang et al., 2012; Zhao et al., 2016; Hua et al., 2018; Zhang et al., 2020). Conventional LIBs typically use organic electrolytes, which have demonstrated poor rate performance and potential safety hazards. ARLBs can efficiently solve these problems because they are environmentally friendly, highly secure, and inexpensive (Zhu et al., 2016; Lakhnot et al., 2019). Indeed, many cathodes of ARLBs exhibit remarkable electrochemical performance, such as $LiMn_2O_4$ (Manjunatha et al., 2011), $LiFePO_4$ (He et al., 2011), and $LiCoO_2$ (Ruffo et al., 2011).

Compared to cathodes, the restricted performance of anodes cannot meet the need for high-performance from ARLBs. Excellent anode materials are a limiting factor for the development of ARLB. Currently, vanadium oxide [VO_2 (Li et al., 1994)] and vanadate [LiV_3O_8 (Zhao et al., 2011), NaV_3O_8 (Zhou et al., 2013)] have been used as anode materials. Nonetheless, these ARLB anodes have problems such as low capacity, poor cycle stability, and low rate performance. In recent times, the NASCION $LiTi_2(PO_4)_3$ anode for ARLBs has shown great potential because it has a three-dimensional channel and a stable structure (Huang et al., 2015). A NASCION-type structure is marked by an open framework, which accelerates the diffusion of Li^+ ions in crystal. TiO_6 octahedra and PO_4 tetrahedra comprise the $LiTi_2(PO_4)_3$ framework unit. The TiO_6 octahedron is connected to the PO_4 tetrahedron, and the structure contains a large gap channel (Vidal-Abarca et al., 2012). Wessells et al. (2011) fabricated $LiTi_2(PO_4)_3$ and demonstrated its potential as an ARLB anode. Luo and Xia (2009) reported a supercapacitor with $LiTi_2(PO_4)_3$ coated with carbon as the negative electrode, delivering a discharge capacity of 30 mAh g^{-1}.

However, the electrochemical performance of a $LiTi_2(PO_4)_3$-based electrode must be increased to meet the requirements of practical applications. Carbon coating, size reduction, and the introduction of a conductive agent are efficient strategies for boosting performance (Sun et al., 2015). Moreover, lattice doping is available as a means of raising anode performance (Mao et al., 2019). Wang et al. (2017) partly replaced F^- on a PO_4^{3-} site for $LiTi_2(PO_4)_3$ as an ARLB anode, with an energy density of 43.7 Wh Kg^1. Liang et al. (2019) prepared Ga-doped $LiTi_2(PO_4)_3$ film via a hydrothermal method and found favorable capacity and cycling performance. Doping with anions such as F^- and Cl^- can promote the electrokinetics of electrodes by influencing electron configuration, further increasing the electrical and ionic

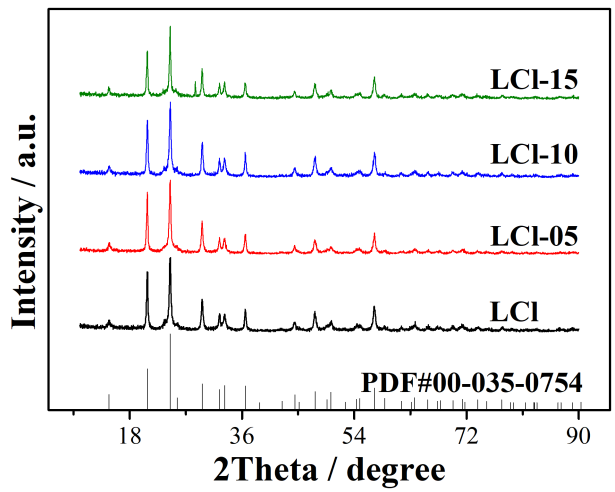

FIGURE 2 | XRD patterns of $NaTi_2(PO_4)_{3-x}Cl_{3x}/C$ (x = 0.0, 0.05, 0.10, and 0.15) composites.

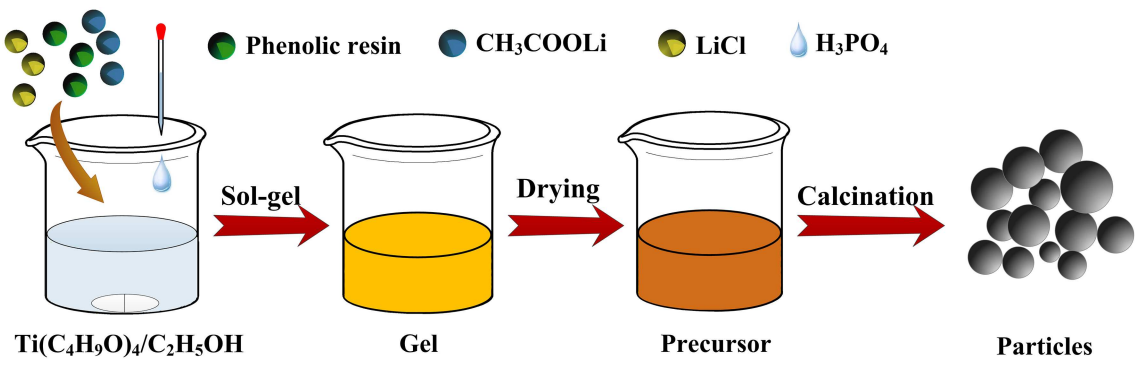

FIGURE 1 | Schematic illustration of the preparation process of the composites.

conductivity (Yue et al., 2013; Qi et al., 2015). In this paper, a Cl^{-1} doping strategy was employed to boost the lithium storage performance of $LiTi_2(PO_4)_3$/C. $LiTi_2(PO_4)_{3-x}Cl_{3x}$/C composites were successfully prepared with a facile sol-gel method. The lithium ion storage performance of anion-doped composites was systematically studied.

EXPERIMENTAL

Synthesis

All analytically pure chemical reagents were directly used without further treatment. The synthesis process of the materials is illustrated in **Figure 1**. Pristine $LiTi_2(PO_4)_3$/C was synthesized via a sol-gel technique as follows. Briefly, 1.7921 g of $Ti(OC_4H_9)_4$ was added to 20 mL of C_2H_5OH, and the $Ti(OC_4H_9)_4/C_2H_5OH$ solution was kept at room temperature with magnetic stirring. Then, 0.2659 g of $CH_3COOLi{\cdot}2H_2O$ and 0.1700 g of phenolic resin were dissolved in the mixture, sequentially. Following this, 0.8924 g of concentrated H_3PO_4 was added into 15 mL of C_2H_5OH and added dropwise to the above mixed solution. The mixed solution was reacted in a sealed beaker at 60°C for 2 h with magnetic stirring. When the reaction was complete, the solution was evaporated at 80°C to obtain a precursor. Finally, the precursor was calcined at 750°C for 5 h in an Ar atmosphere; the prepared $LiTi_2(PO_4)_3$/C was named LCl. Moreover, $LiTi_2(PO_4)_{3-x}Cl_{3x}$/C ($x = 0.05$, 0.10, and 0.15) composites were synthesized by partially replacing PO_4^{3-} with Cl^- in stoichiometry with LiCl. The corresponding $LiTi_2(PO_4)_{3-x}Cl_x$/C composites were denoted as LCl-05, LCl-10, and LCl-15.

Characterizations

X-ray powder diffraction (XRD, D/MAX2500PC, Rigaku) was carried out to analyze the crystalline phase of the composites. A scanning electron microscope (S-4800, Japan) was used to investigate the morphology of the samples and cycled electrodes. Cycled electrodes were obtained after disassembling the cells, washing them with deionized water, and drying them in an oven. A thermal analyzer (TG50, Shimadzu) was used for thermogravimetric analysis (TGA) of the samples.

Electrochemical Measurements

The electrodes were prepared as follows. The electrodes consisted of an intermixture of acetylene black, active substance, and PTFE (mass ratio: 1:1:8). The intermixture was pressed on a steel mesh with a radius of 7 mm. In cells, $LiMn_2O_4$, the synthesized samples, a saturated Li_2SO_4 solution, and glass fiber were used as the cathode, anode, electrolyte, and separator, respectively. A galvanostatic charge-discharge test for the cells was executed on a CT2001A testing system. Rate performance was evaluated at 0.2, 0.5, 1, 2, 5, 8, 10, 15, and 1°C, respectively. The cycling performance was recorded under 5°C for 1,000 cycles. Cyclic voltammetry and electrochemical impedance spectroscopy were performed to explore the lithium ion storage performance of Li^+ ions using a CHI660E electrochemical workstation (Chenhua,

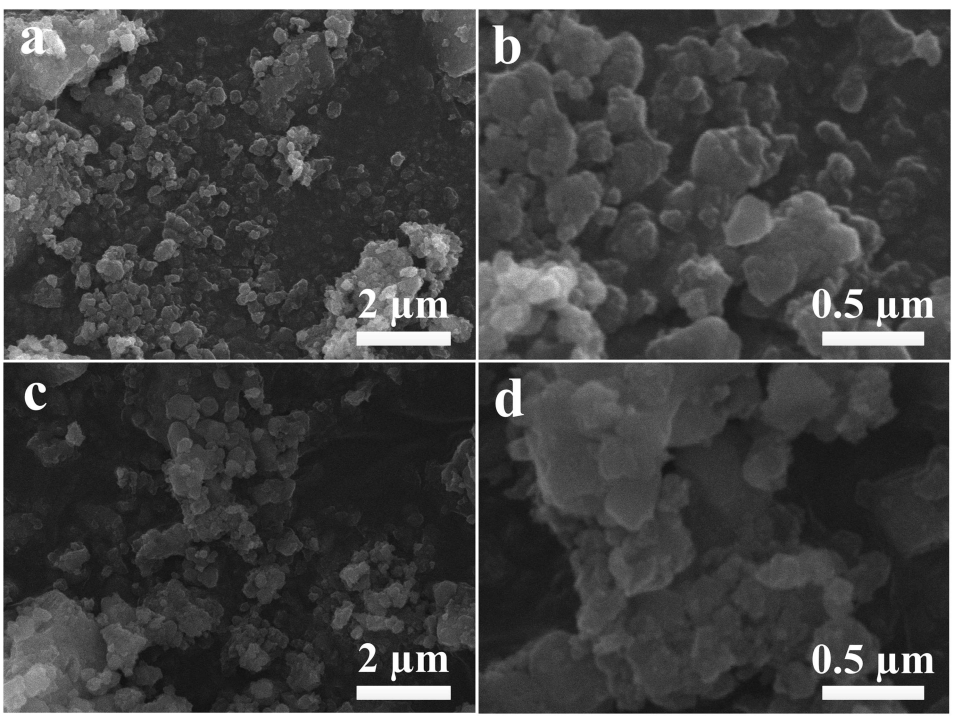

FIGURE 3 | SEM images of LCl **(a,b)** and LCl-10 **(c,d)** at different magnifications.

Shanghai). Cyclic voltammetry tests were executed with a voltage range of 0–1.85 V. Electrochemical impedance spectroscopy tests for electrochemically activated cells were conducted with a frequency of 10^5-10^{-2} Hz and an amplitude of 5 mV.

RESULTS AND DISCUSSION

The XRD patterns of the composites are presented in **Figure 2**. As shown, the main characteristic peaks of all composites were similar and exactly matched those of the NASICON $LiTi_2(PO_4)_3$ with an R-3c space group (JCPDS#35-0754). This demonstrated that doping with small amount of Cl had no effect on the main structure of $LiTi_2(PO_4)_3$. In addition, LCl-15 showed an impurity peak at 28.4 degrees, which demonstrated that a high Cl content slightly influenced the crystal structure of Cl-doped composites.

Representative SEM images of LCl and LCl-10 at various magnifications are displayed in **Figure 3**. As displayed, both materials were constituted by tiny primary particles at a nanometer scale. In addition, there was some agglomeration resulting from the high temperatures reached during the synthesis process. As for the morphology of the LCl-10 composite, it exhibited no obvious differences compared to pristine LCl, further implying that Cl doping had no obvious impact on the composite morphology.

The rate performance of the composites is shown in **Figure 4A**. Serious electrochemical polarization in a large current resulted in a decrease in the discharge capacity of all composites as the rate increased. The discharge capacity of Cl-doped $LiTi_2(PO_4)_3$ composites, particularly LCl-10, was increased compared to the original $LiTi_2(PO_3)_4$/C, indicating an improvement with Cl-doped anode materials. The difference in discharge capacity between Cl-doped $LiTi_2(PO_4)_3$ composites and the original $LiTi_2(PO_3)_4$/C became more obvious as the rate was increased. LCl-10 delivered a discharge capacity of 108.5 and 85.5 mAh g^{-1} at 0.5 and 15°C, respectively, an increase of 13.1 and 44.3 mAh g^{-1} compared to pristine LCl. Charge-discharge curves for the LCl and LCl-10 composites at disparate rates are displayed in **Figures 4B,C**, respectively. There were two voltage plateaus for LCl and LCl-10, at about 1.0 and 1.5 V. The voltage plateaus of LCl-10 were wider and more stable compared to those of LCl, revealing the outstanding electrochemical performance of LCl-10.

The cycling properties of LCl and LCl-10 composites were studied at 5°C for 1,000 cycles, and the results are shown in **Figure 5A**. The discharge capacity of both composites gradually increased during the first several cycles due to electrode activation. The maximal discharge capacity of LCl-10 (95.27 mAh g^{-1}) was higher than that of LCl (84.89 mAh g^{-1}). The discharge capacity of LCl-10 was maintained at 61.3% after 1,000 cycles, which was 25.1% higher than that of LCl (36.2%). **Figure 5B** shows that the coulombic efficiencies of LCl and LCl-10 were in the vicinity of 100%, revealing that the cells had almost no self-discharge. The charge-discharge curves for LCl and LCl-10 after various cycles are shown in **Figures 5C,D**, respectively. The relatively wider and more stable voltage plateau for

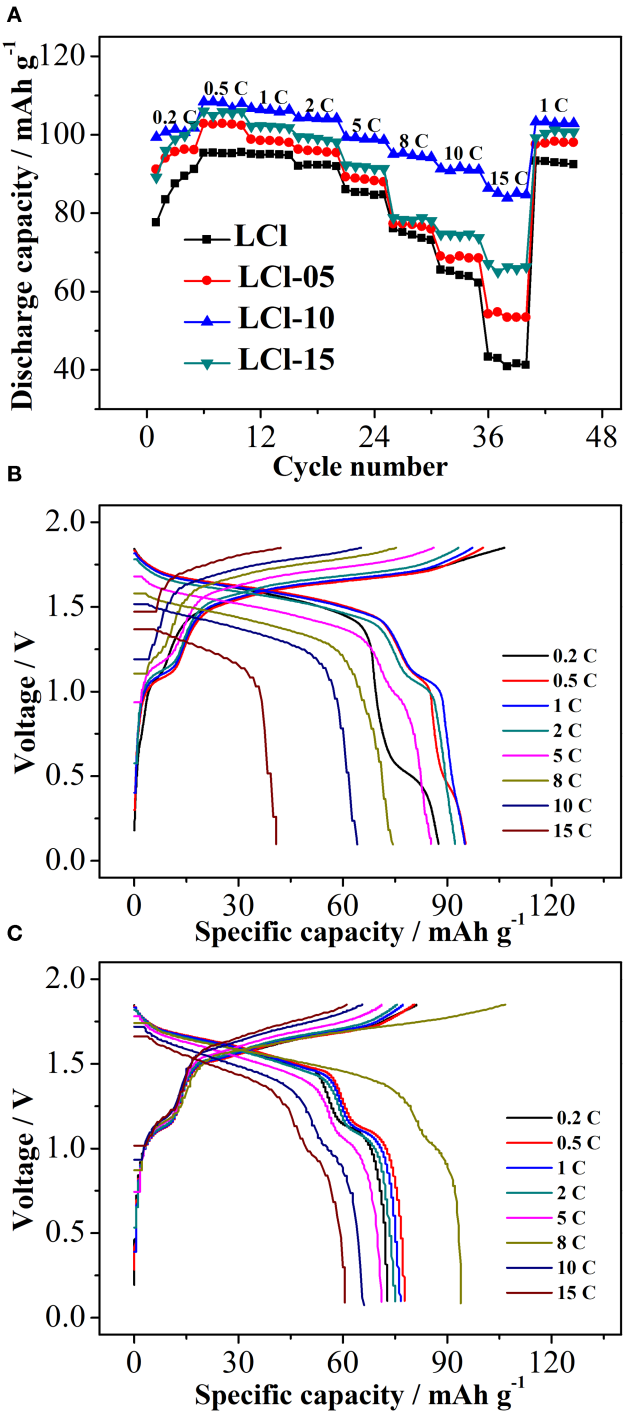

FIGURE 4 | Rate performance of all composites **(A)**, charge-discharge curves for LCl **(B)** and LCl-10 **(C)** at different rates.

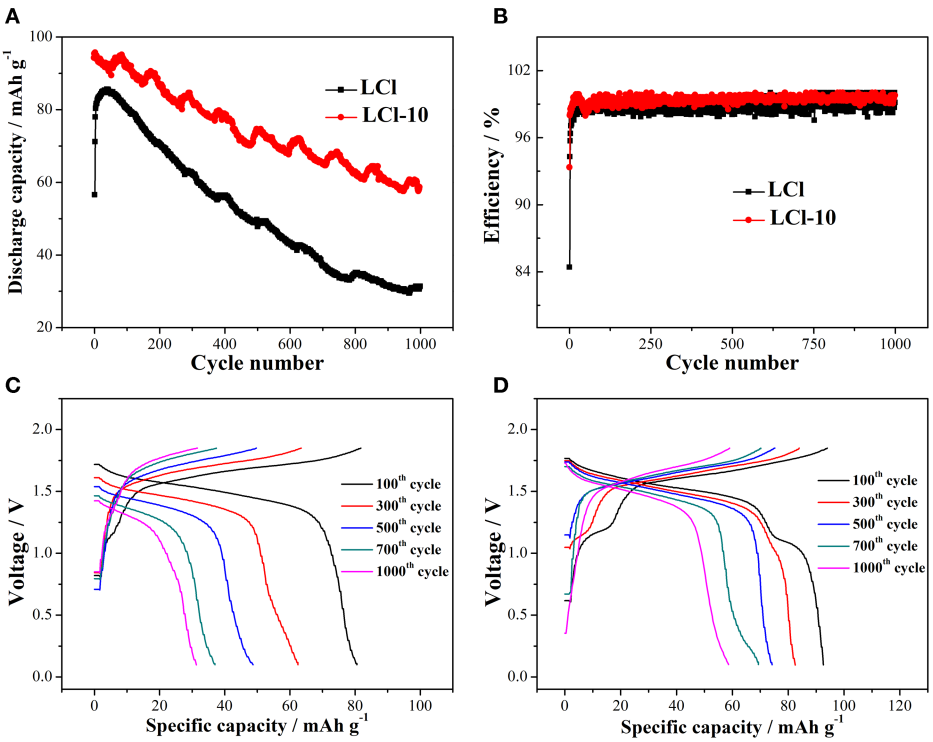

FIGURE 5 | Cycling performances **(A)** and coulombic efficiency **(B)** for LCl and LCl-10 at 5°C for 1,000 cycles, charge-discharge curves for LCl **(C)** and LCl-10 **(D)** after different cycles.

LCl-10 demonstrated good electrochemical performance and stability, unveiling the remarkable cycling properties of LCl-10.

In order to study the structural stability of the electrode after multiple cycles, the electrode morphology was analyzed by SEM. The results for LCl-10 electrodes after 100, 500, and 1,000 cycles are shown in **Figure 6**. As can be seen, the LCl-10 electrode surface was smooth after 100 cycles, and the morphology remained stable even after 1,000 cycles, without apparent dissolution. This demonstrated that LCl-10 had excellent structural stability after a long period of charging and discharging.

Cyclic voltammetry tests of the cells for LCl and LCl-10 were carried out to study the electrochemical kinetics, and the results are shown in **Figure 7**. As can be observed, both LCl and LCl-10 had two obvious current peaks. Further, the current density of LCl-10 was higher than the corresponding current density of LCl. The higher current density and narrower peak potential difference of LCl-10 illustrated the excellent electrochemical property of LCl-10. The anodic and cathodic peak current density of LCl-10 at 1.6 V reached 0.38 and 0.38 A g^{-1}, respectively, with an obvious improvement compared to LCl (0.30 and 0.30 A g^{-1}). The peak potential difference of LCl-10 with a value of 0.12 V was smaller than that of LCl (0.15 V), indicating better electrochemical reversibility of the modified electrode.

An electrochemical impedance spectroscopy test was implemented to investigate the effect of Cl doping on the electrochemical kinetics. Nyquist plots and fitting results for LCl and LCl-10 are shown in **Figure 8**. The Nyquist plots were characterized by an intercept, a semicircle, and an inclined line at high, middle, and low frequencies, parallel to ohmic resistance (R_s) including the electrolyte and electrode, charge transfer resistance (R_{ct}) linked with the electrochemical reaction, and Warburg impedance (Z_w) related to the migration of Li ions, respectively. As can be seen, the electronic conductivity of LCl-10 did not change significantly compared to that of LCl. This indicated that Cl doping caused no obvious change in the electronic conductivity of the material. This was due to the improvement in electronic conductivity from the introduction of carbon. LCl-10 delivered an R_{ct} value of 30.0 Ω, which was less than that of LCl (43.9 Ω), illustrating that the Cl doping had a positive effect on the electrochemical kinetics.

CONCLUSIONS

$LiTi_2(PO_4)_3$/C composites doped with chlorine on phosphate spots were successfully synthesized with a sol-gel technique. Chlorine doping did not significantly impact the main

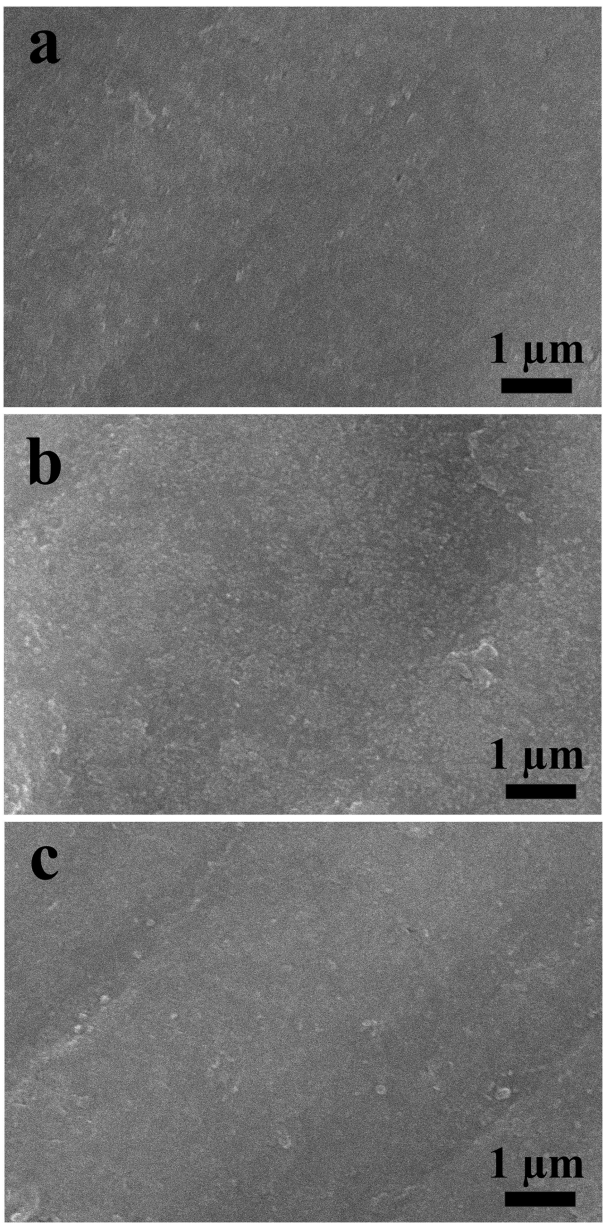

FIGURE 6 | SEM images of LCl-10 anodes after 100 **(a)**, 500 **(b)**, and 1,000 **(c)** cycles at a rate of 5°C.

structure and morphology of $LiTi_2(PO_4)_3$/C. Of all the samples, LCL-10 composites showed the optimum rate performance, and their advantages were more obvious at a higher rate. LCl-10 had a discharge capacity of 108.5 and 85.5 mAh g^{-1} at 0.5 and 15°C, respectively, which was 13.1 and 44.3 mAh g^{-1} higher than those of LCl. Moreover, the discharge capacity of LCl-10 was maintained at 61.3% after 1,000 cycles at 5°C, which was 25.1% higher than that of LCl (36.2%). In a word, $LiTi_2(PO_4)_3$/C doped with an appropriate amount of chlorine is a potential anode for high-performance ARLBs.

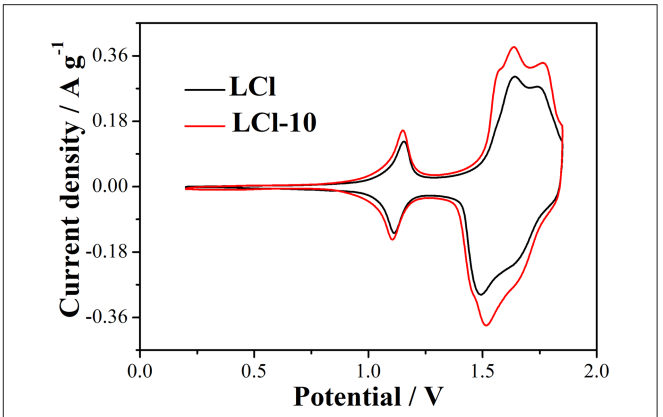

FIGURE 7 | Cyclic voltammetry curves of the cells using LCl and LCl-10 at a scan rate of 0.5 mV s^{-1}.

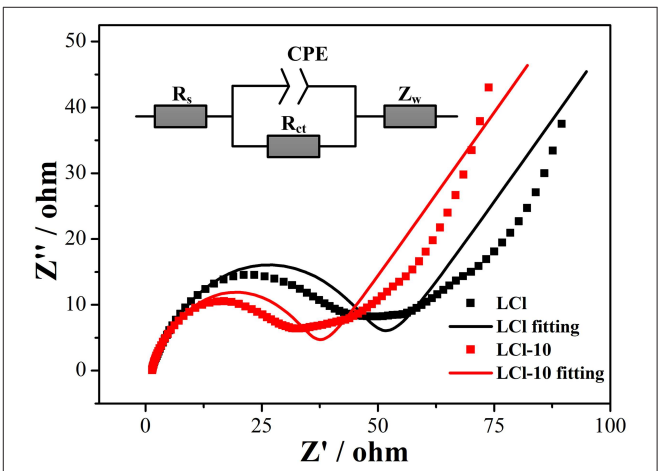

FIGURE 8 | Electrochemical impedance spectra and fitting results of the assembled cell for LCl and LCl-10.

DATA AVAILABILITY STATEMENT

All datasets generated for this study are included in the article/supplementary material.

AUTHOR CONTRIBUTIONS

HL: carried out experiments and wrote the manuscript. YT: carried out experiments. ZX: performed analyzed experimental results. PW: designed experiments. ZL: revised the manuscript.

FUNDING

This research was funded by the National Natural Science Foundation of China (NNSFC), grant numbers 11704223 and 11803015, by the Natural Science Foundation of Fujian Province, grant number 2018J05008 and JZ160459, by the Ph.D. Research Startup Foundation of Quanzhou Normal University (G16057), and by the Distinguished Young Scholars Program of Fujian Province (C18032).

REFERENCES

Fang, Y. Z., Hu, R., Liu, B. Y., Zhang, Y. Y., Zhu, K., Yan, J., et al. (2019). MXene-derived TiO_2/reduced graphene oxide composite with an enhanced capacitive capacity for Li-ion and K-ion batteries. *J. Mater. Chem. A* 7, 5363–5372. doi: 10.1039/C8TA12069B

He, D., Huang, X., and Li, M. (2019). Hierarchical $CP(=O)(O)_n$ ($n \leq 2$)-linked nano-Si/N-doped C/graphene porous foam as anodes for high-performance lithium ion batteries. *Carbon* 141, 531–541. doi: 10.1016/j.carbon.2018.10.007

He, P., Liu, J. L., Cui, W. J., Luo, J. Y., and Xia, Y. Y. (2011). Investigation on capacity fading of $LiFePO_4$ in aqueous electrolyte. *Electrochim Acta* 56, 2351–2357. doi: 10.1016/j.electacta.2010.11.027

Hua, K., Li, X., Fang, D., Bao, R., Yi, J., Luo, Z., et al. (2018). Vanadium trioxide nanowire arrays as a cathode material for lithium-ion battery. *Ceram Int.* 44, 11307–11313. doi: 10.1016/j.ceramint.2018.03.178

Huan, H., Jile, H., Tang, Y. J., Li, X., Yi, Z., Gao, X., et al. (2020). Fabrication of $ZnO@Ag@Ag_3PO_4$ ternary heterojunction: superhydrophilic properties, antireflection and photocatalytic properties. *Micromachines* 11:309. doi: 10.3390/mi11030309

Huang, Z., Liu, L., Zhou, Q., Tan, J., Yan, Z., Xia, D., et al. (2015). Carbon-coated lithium titanium phosphate nanoporous microplates with superior electrochemical performance. *J. Power Sources* 294, 650–657. doi: 10.1016/j.jpowsour.2015.06.143

Jiang, S. L., Huang, R. M., Zhu, W. C., Li, X. Y., Zhao, Y., Gao, Z. X., et al. (2019). Free-Standing SnO_2@rGO anode via the anti-solvent-assisted precipitation for superior lithium storage performance. *Front. Chem.* 7:878. doi: 10.3389/fchem.2019.00878

Lakhnot, A. S., Gupta, T., Singh, Y., Hundekar, P., Jain, R., Han, F., et al. (2019). Aqueous lithium-ion batteries with niobium tungsten oxide anodes for superior volumetric and rate capability. *Energy Storage Mater* 27, 506–513. doi: 10.1016/j.ensm.2019.12.012

Li, J. K., Chen, X. F., Yi, Z., Yang, H., Tang, Y. J., Yi, Y., et al. (2020a). Broadband solar energy absorber based on monolayer molybdenum disulfide using tungsten elliptical arrays. *Mater. Today Energy* 16:100390. doi: 10.1016/j.mtener.2020.100390

Li, J. K., Chen, Z. Q., Yang, H., Yi, Z., Chen, X. F., Yao, W. T., et al. (2020b). Tunable broadband solar energy absorber based on monolayer transition metal dichalcogenides materials using au nanocubes. *Nanomaterials* 10:257. doi: 10.3390/nano10020257

Li, W., McKinnon, W. R., and Dahn, J. R. (1994). Lithium intercalation from aqueous solutions. *J. Electrochem. Soc.* 141, 2310–2316. doi: 10.1149/1.2055118

Liang, Y., Peng, C., Kamiike, Y., Kuroda, K., and Okido, M. (2019). Gallium doped NASICON type $LiTi_2(PO_4)_3$ thin-film grown on graphite anode as solid electrolyte for all solid state lithium batteries. *J. Alloy Compd.* 775, 1147–1155. doi: 10.1016/j.jallcom.2018.10.226

Lu, M., Zhang, X., Ji, J., Xu, X., and Zhang, Y. (2020). Research progress on power battery cooling technology for electric vehicles. *J. Energy Storage* 27:101155. doi: 10.1016/j.est.2019.101155

Luo, J. Y., and Xia, Y.-Y. (2009). Electrochemical profile of an asymmetric supercapacitor using carbon-coated $LiTi_2(PO_4)_3$ and active carbon electrodes. *J. Power Sources* 186, 224–227. doi: 10.1016/j.jpowsour.2008.09.063

Manjunatha, H., Mahesh, K. C., Suresh, G. S., and Venkatesha, T. V. (2011). The study of lithium ion de-insertion/insertion in $LiMn_2O_4$ and determination of kinetic parameters in aqueous Li_2SO_4 solution using electrochemical impedance spectroscopy. *Electrochim Acta* 56, 1439–1446. doi: 10.1016/j.electacta.2010.08.107

Mao, Q., Zhang, C., Yang, W., Yang, J., Sun, L., Hao, Y., et al. (2019). Mitigating the voltage fading and lattice cell variations of O3-$NaNi_{0.2}Fe_{0.35}Mn_{0.45}O_2$ for high performance Na-ion battery cathode by Zn doping. *J. Alloy Compd.* 794, 509–517. doi: 10.1016/j.jallcom.2019.04.271

Qi, Y., Mu, L., Zhao, J., Hu, Y.-,S., Liu, H., and Dai, S. (2015). Superior Na-storage performance of low-temperature-synthesized $Na_3(VO_{1-x}PO_4)_2F_{1+2x}$ ($0 \leq x \leq 1$) Nanoparticles for Na-ion batteries. *Angew. Chem. Int. Ed.* 54, 9911–9916. doi: 10.1002/anie.201503188

Ruffo, R., La Mantia, F., Wessells, C., Huggins, R. A., and Cui, Y. (2011). Electrochemical characterization of $LiCoO_2$ as rechargeable electrode in aqueous $LiNO_3$ electrolyte. *Solid State Ionics* 192, 289–292. doi: 10.1016/j.ssi.2010.05.043

Sun, D., Xue, X., Tang, Y., Jing, Y., Huang, B., Ren, Y., et al. (2015). High-rate $LiTi_2(PO_4)_3$@N-C composite via bi-nitrogen sources doping. *ACS Appl. Mater. Inter.* 7, 28337–28345. doi: 10.1021/acsami.5b08697

Vidal-Abarca, C., Lavela, P., Aragon, M. J., Plylahan, N., and Tirado, J. L. (2012). The influence of iron substitution on the electrochemical properties of $Li_{1+x}Ti_{2-x}Fe_x(PO_4)_3$/C composites as electrodes for lithium batteries. *J. Mater. Chem.* 22, 21602–21607. doi: 10.1039/c2jm34227h

Wang, H. Q., Zhang, H. Z., Cheng, Y., Feng, K., Li, X. F., and Zhang, H. M. (2017). Rational design and synthesis of $LiTi_2(PO_4)_{3-x}F_x$ anode materials for high-performance aqueous lithium ion batteries. *J. Mater. Chem. A* 5, 593–599. doi: 10.1039/C6TA08257B

Wang, Y., Yi, J., and Xia, Y. (2012). Recent progress in aqueous lithium-ion batteries. *Adv. Energy Mater.* 2, 830–840. doi: 10.1002/aenm.201200065

Wessells, C., Huggins, R. A., and Cui, Y. (2011). Recent results on aqueous electrolyte cells. *J. Power Sources* 196, 2884–2888. doi: 10.1016/j.jpowsour.2010.10.098

Wu, X., Xiang, Y., Peng, Q., Wu, X., Li, Y., Tang, F., et al. (2017). Green-low-cost rechargeable aqueous zinc-ion batteries using hollow porous spinel $ZnMn_2O_4$ as the cathode material. *J. Mater. Chem. A* 5, 17990–17997. doi: 10.1039/C7TA00100B

Yang, S. N., Zhang, M. S., Wu, X. W., Wu, X. S., Zeng, F. H., Li, Y. T., et al. (2019). The excellent electrochemical performances of $ZnMn_2O_4/Mn_2O_3$: The composite cathode material for potential aqueous zinc ion batteries. *J. Electroanal Chem.* 832, 69–74. doi: 10.1016/j.jelechem.2018.10.051

Yue, P., Wang, Z., Li, X., Xiong, X., Wang, J., Wu, X., et al. (2013). The enhanced electrochemical performance of $LiNi_{0.6}Co_{0.2}Mn_{0.2}O_2$ cathode materials by low temperature fluorine substitution. *Electrochim Acta* 95, 112–118. doi: 10.1016/j.electacta.2013.02.037

Zhang, C., Zheng, B., Song, Z., Shi, S., and Mao, H. (2020). Microwave-assisted synthesis of a novel $CuC_2O_4 \cdot xH_2O$/Graphene composite as anode material for lithium ion batteries. *Ceram Int.* 46, 1018–1025. doi: 10.1016/j.ceramint.2019.09.066

Zhao, M., Zheng, Q., Wang, F., Dai, W., and Song, X. (2011). Electrochemical performance of high specific capacity of lithium-ion cell LiV_3O_8//$LiMn_2O_4$ with $LiNO_3$ aqueous solution electrolyte. *Electrochim Acta* 56, 3781–3784. doi: 10.1016/j.electacta.2011.02.057

Zhao, R., Liu, J., and Gu, J. (2016). Simulation and experimental study on lithium ion battery short circuit. *Appl. Energy* 173, 29–39. doi: 10.1016/j.apenergy.2016.04.016

Zhou, D., Liu, S., Wang, H., and Yan, G. (2013). $Na_2V_6O_{16}\bullet 0.14H_2O$ nanowires as a novel anode material for aqueous rechargeable lithium battery with good cycling performance. *J. Power Sources* 227, 111–117. doi: 10.1016/j.jpowsour.2012.11.022

Zhou, P., Zhang, M. Y., Wang, L. P., Huang, Q. Z., Su, Z. A., Li, L. W., et al. (2019). Synthesis and electrochemical performance of ZnSe electrospinning nanofibers as an anode material for lithium ion and sodium ion batteries. *Front. Chem.* 7:569. doi: 10.3389/fchem.2019.00569

Zhu, Q., Zheng, S., Lu, X., Wan, Y., Chen, Q., Yang, J., et al. (2016). Improved cycle performance of $LiMn_2O_4$ cathode material for aqueous rechargeable lithium battery by LaF_3 coating. *J. Alloy Compd.* 654, 384–391. doi: 10.1016/j.jallcom.2015.09.085

Conflict of Interest: The authors declare that the research was conducted in the absence of any commercial or financial relationships that could be construed as a potential conflict of interest.